Biology of Reproduction, 2020, 102(5), 1055–1064
doi:10.1093/biolre/ioaa008
Research Article
Advance Access Publication Date: 13 January 2020

OXFORD

Research Article

Inactivation of TRP53, PTEN, RB1, and/or CDH1 in the ovarian surface epithelium induces ovarian cancer transformation and metastasis

Mingxin Shi[1], Allison E. Whorton[1], Nikola Sekulovski[1], Marilène Paquet[2], James A. MacLean II[1], Yurong Song[3], Terry Van Dyke[3] and Kanako Hayashi[1,*]

[1]Department of Physiology, Southern Illinois University School of Medicine, Carbondale, Illinois, USA; [2]Departement de Pathologie et de Microbiologie, Université de Montreal, St-Hyacinthe, Quebec, Canada [3]Mouse Cancer Genetics Program, Center for Cancer Research, National Cancer Institute, Frederick, Maryland, USA

***Correspondence**: Department of Physiology, Southern Illinois University School of Medicine, 1135 Lincoln Dr., Carbondale, Illinois, USA. Tel: 618-453-1562, Fax: 618-453-1517, E-mail khayashi@siumed.edu

Received 26 November 2019; Revised 24 December 2019; Accepted 9 January 2020

Abstract

Ovarian cancer (OvCa) remains the most common cause of death from gynecological malignancies. Genetically engineered mouse models have been used to study initiation, origin, progression, and/or mechanisms of OvCa. Based on the clinical features of OvCa, we examined a quadruple combination of pathway perturbations including PTEN, TRP53, RB1, and/or CDH1. To characterize the cancer-promoting events in the ovarian surface epithelium (OSE), *Amhr2*$^{cre/+}$ mice were used to ablate floxed alleles of *Pten*, *Trp53,* and *Cdh1*, which were crossed with TgK19GT$_{121}$ mice to inactivate RB1 in KRT19-expressing cells. Inactivation of PTEN, TRP53, and RB1 with or without CDH1 led to the development of type I low-grade OvCa with enlarged serous papillary carcinomas and some high-grade serous carcinomas (HGSCs) in older mice. Initiation of epithelial hyperplasia and micropapillary carcinoma started earlier at 1 month in the triple mutations of *Trp53*, *Pten*, and *Rb1* mice as compared to 2 months in quadruple mutations of *Trp53*, *Pten*, *Rb1*, and *Cdh1* mice, whereas both genotypes eventually developed enlarged proliferating tumors that invaded into the ovary at 3–4 months. Mice with triple and quadruple mutations developed HGSC and/or metastatic tumors, which disseminated into the peritoneal cavity at 4–6 months. In summary, inactivation of PTEN, TRP53, and RB1 initiates OvCa from the OSE. Additional ablation of CDH1 further increased persistence of tumor dissemination and ascites fluid accumulation enhancing peritoneal metastasis.

Summary sentence

Inactivation of TRP53, PTEN, and RB1 initiates ovarian cancer from the ovarian surface epithelium. Additional ablation of CDH1 further increased persistence of tumor dissemination.

Key words: PTEN, TRP53, CDH1, RB1 and epithelial ovarian cancer

Introduction

Ovarian cancer (OvCa) remains the most common cause of death from gynecological malignancies and is the fifth leading overall cause of death from cancer in women. In 2019, approximately 22,500 new OvCa cases and 14,000 deaths were estimated from OvCa in the United States [1]. The majority of OvCa (85–90%) is histologically classified as epithelial ovarian cancer (EOC) [2, 3]. They are further divided into type I, low-grade OvCa and type II, high-grade aggressive malignancies based on the clinical behavior and histopathological types of EOC [3, 4]. Most type II malignancies

feature high-grade serous carcinomas (HGSCs), which have a high propensity for metastasis, resulting in low overall survival [3]. The cancer genome landscape of HGSC has unequivocally reported that 96% of HGSCs harbor mutations of *TP53* [5]. These studies have also highlighted alterations in the RB1 pathway (67%), the phosphoinositide 3-kinase (PI3K) pathway (45%), and Notch signaling (22%) in HGSC [5]. Although OvCa is a complex heterogeneous disease, a clear understanding of molecular pathogenesis in OvCa is necessary for early stage diagnosis as well as rational design of therapies.

Genetically engineered mouse models of OvCa have been developed to understand the specific functions of oncogenes and/or tumor suppressors and the etiology of OvCa formation [3, 6–8]. Via deletion of regulatory floxed genes by injecting adenovirus-Cre to the ovarian bursa and/or crossing with $Amhr2^{cre/+}$ mice, the ovarian surface epithelium (OSE) can be transformed into OvCa. Specifically, combination of *Pten*, $Kras^{G12D}$, and/or $Trp53^{R172H}$ mutation by $Amhr2^{cre/+}$ mice can induce EOC such as serous papillary adenocarcinomas, mucinous with serous features of carcinomas and/or HGSC [9–11]. On the other hand, recent evidence, from clinical and animal studies of OvCa, shows that HGSCs appear to arise from the fallopian tube epithelium (FTE) [3]. The use of *Pax8* or *Ovgp1* promoters to express Cre recombinase enables to target/disrupt genes in FTE [12–15] resulting in the induction of HGSC and serous tubal intraepithelial carcinomas mimicking the development of OvCa [12, 14]. While each model will provide some similarities and differences in the clinical features and molecular aspects of OvCa, genetically engineered mice with deletion or inactivation of tumor suppressor genes and/or exogenous expression of oncogenes in a tissue-specific manner provide a better understanding of the molecular mechanisms in the precise origin of cells in OvCa.

In the present study, we have generated a mouse model of OvCa in which *Trp53*, *Pten*, and/or RB1, well-known altered signaling pathways in OvCa, were conditionally ablated or inactivated in the OSE using $Amhr2^{cre/+}$ mice. We have also induced disruption of epithelial cells by deleting *Cdh1* with a combination of *Trp53*, *Pten*, and/or RB1 in OSE to examine the importance of epithelial structure of OSE. While *CDH1* mutation and/or deletion is not common (~5%) in OvCa based on datasets from The Cancer Genome atlas Program (TCGA), physical disruption of epithelial cells in the OSE can be routinely induced by ovulation. Increased ovulations with damaged OSE could serve as the origin of OvCa [3, 16]. In addition, CDH1 ablation is one of the progressive phenomena in cancer metastasis [17–19]. Inactivation of TRP53, PTEN, and RB1 in the OSE was predicted to induce type I low-grade OvCa such as papillary features of adenocarcinomas with some HGSC phenotype and metastasis. The combined inactivation of TRP53, PTEN, and RB1 in the OSE resulted in loss of normal epithelial characteristics. Interestingly, loss of *Cdh1* seemed to cause disruption in the epithelial histoarchitecture that delayed the onset of OvCa and elicited poorly differentiated ovarian tumors. However, after OvCa establishment, these mice exhibited poor survivability and all succumbed to the disease by 6.5 months.

Materials and methods

Animals and tissue collection

Mice were maintained in the vivarium at Southern Illinois University according to the institutional guidelines for the care and use of laboratory animals (protocol #16–038). Health of mice was continuously monitored by investigators and vivarium staff according to National Research Council guidelines [20]. Mice with tumor burden precluding normal movement and access to food/water were euthanized and the day of sacrifice recorded. *B6.129-*$Amhr2^{tm3(cre)Bbr}$ (aka $Amhr2^{cre/+}$) mice were provided by Dr. Richard R. Behringer (Univ. Texas MD Anderson Cancer Center [21]). *B6.129-*$Cdh1^{tmKem2}$/J (aka $Cdh1^{flox}$, Jax #005319) and *B6.129S4-*$Pten^{tm1Hwu}$ (aka $Pten^{flox}$, Jax #006440) mice were obtained from the Jackson Laboratory. *FVB.129-*$Trp53^{tm1Brn}$ (aka $Trp53^{flox}$, #01XC2) mice were obtained from the Mouse Models of Human Cancers Consortium, NIH. *B6.D2-Tg(K19GT*$_{121}$*)Tvd* (aka $TgK19GT_{121}$) mice were obtained from Drs. Yurong Song and Terry van Dyke [22, 23]. Tissues were collected at 1, 2, 3, 4, and 6 months, and were fixed in fresh 4% paraformaldehyde in PBS at room temperature and embedded in paraffin, or homogenized with Trizol (Thermo Fisher, Waltham, MA) for RNA extraction.

Histology and immunohistochemistry

Tissue sections were stained with haematoxylin and eosin (H&E) and evaluated by Marilène Paquet, a board-certified pathologist according to current ovarian cancer pathogenesis [3, 4, 24]. At least five sections were examined for each genotype or time point. Immunolocalization of Ki67, KRT14, CDH1, PAX8, WT1, SV40 T Antigen (RB1), and PTEN was determined in cross-sections (5 µm) of paraffin-embedded tissue sections using specific primary antibodies and a Vectastain Elite ABC Kit (Vector laboratories, Burlingame, CA, USA). Primary antibodies used in these analyses were anti-Ki67 (1:250 dilution, 550609, BD Biosciences, San Jose, CA); KRT14 (1:200 dilution, PIPA532460, Invitrogen, Waltham, MA); anti-CDH1 (1:250 dilution, 610181, BD Biosciences); PAX8 (1:200 dilution, 10336–1-AP, Proteintech, Rosemont, IL); anti-WT1 (1:200 dilution, ab89901, Abcam, Cambridge, MA); anti-SV40 T Antigen (1:150 dilution, DP02, Millipore Sigma, St. Louis, MO); and PTEN (1:250 dilution, 9552, Cell Signaling Technology, Danvers, MA).

Quantitative real-time PCR analysis (QPCR)

Total RNA was isolated from the tissues, and cDNA was synthesized from total RNA using the High-Capacity cDNA Reverse Transcription Kit (Thermo Fisher, USA). Relative gene expression was determined by SYBR green (Bio Rad, USA) incorporation using a Bio-Rad CFX as described previously [25]. Primer sequences were determined using NCBI's design tools and are provided in Supplementary Table S1.

Statistical analysis

Graphs were constructed and statistics were analyzed with GraphPad Prism 5.0 (GraphPad, San Diego, CA). Overall survival rates were determined by Kaplan–Meier analysis and P-value was determined by log-rank test. Student's t-test was used to compare the relative *Trp53* mRNA expression levels between control and $Trp53^{d/d}$ mice. Tests of significance were performed using the appropriate error terms according to the expectation of the mean squares for error. A *P*-value of 0.05 or less was considered significant.

Results

Generation of mice with Pten, Trp53, and Cdh1 ablation and RB1 inactivation in the mouse ovary

To characterize the cancer-promoting events in the ovary, $Amhr2^{Cre/+}$ mice were crossed with $Pten^{f/f}$, $Trp53^{f/f}$, $Cdh1^{f/f}$, and/or $TgK19GT_{121}$ mice to provide a tissue-specific ablation/inactivation of PTEN, TRP53, CDH1, and/or RB1 in *Amhr2*-expressing cells. $TgK19GT_{121}$

mice can Cre-dependently inactivate RB1 in KRT19 (cytokeratin 19)-expressing cells. T_{121} is comprised of the first 121 amino acids of the SV40 large T antigen and inactivates RB1 and its functionally redundant proteins RBL1 (p107) and RBL2 (p130) (see details in [22, 23]). *Amhr2*$^{+/+}$*Pten*$^{f/f}$ *Trp53*$^{f/f}$ *Cdh1*$^{f/f}$ *TgK19GT*$_{121}$ = Control, *Amhr2*$^{Cre/+}$*Pten*$^{f/f}$ *Trp53*$^{+/+}$ *Cdh1*$^{+/+}$ = *Pten*$^{d/d}$, *Amhr2*$^{Cre/+}$*Pten*$^{+/+}$ *Trp53*$^{f/f}$ *Cdh1*$^{+/+}$ = *Trp53*$^{d/d}$, *Amhr2*$^{Cre/+}$*Pten*$^{+/+}$ *Trp53*$^{+/+}$ *Cdh1*$^{f/f}$ = *Cdh1*$^{d/d}$, *Amhr2*$^{Cre/+}$*Pten*$^{+/+}$ *Trp53*$^{+/+}$ *Cdh1*$^{+/+}$ *TgK19GT*$_{121}$ = *TgK19GT*$_{121}$, *Amhr2*$^{Cre/+}$*Pten*$^{f/f}$ *Trp53*$^{f/f}$ *Cdh1*$^{+/+}$ = *Pten*$^{d/d}$ *Trp53*$^{d/d}$, *Amhr2*$^{Cre/+}$*Pten*$^{f/f}$ *Trp53*$^{f/f}$ *Cdh1*$^{f/f}$ = *Pten*$^{d/d}$ *Trp53*$^{d/d}$ *Cdh1*$^{d/d}$, *Amhr2*$^{Cre/+}$*Pten*$^{f/f}$ *Trp53*$^{f/f}$ *Cdh1*$^{+/+}$ *TgK19GT*$_{121}$ = *Pten*$^{d/d}$ *Trp53*$^{d/d}$ *TgK19GT*$_{121}$, and *Amhr2*$^{Cre/+}$*Pten*$^{f/f}$ *Trp53*$^{f/f}$ *Cdh1*$^{f/f}$ *TgK19GT*$_{121}$ = *Pten*$^{d/d}$ *Trp53*$^{d/d}$ *Cdh1*$^{d/d}$ *TgK19GT*$_{121}$. Genotyping by PCR is shown in Figure 1A, and the primers for genotyping are shown in Supplementary Table S1. Cre recombinase in *Amhr2*$^{Cre/+}$ mice is active in the OSE and granulosa cells in the ovary [26], and it is known that *Amhr2*$^{Cre/+}$ mice are able to induce EOC and/or granulosa tumors depending on the target genes [9, 27, 28]. The ability of *Amhr2-Cre* recombinase to mediate ablation of *Trp53*, *Cdh1*, and *Pten* in the ovary was confirmed by *Trp53* mRNA analysis, as well as PTEN and CDH1 (black arrow) immunoreactivity (Figure 1B–D). A floxed eGFP-stop-T_{121} cassette is inserted into exon 1 start codon of KRT19, and RB1 inactivation in KRT-expressing cells has been confirmed in the OSE [22]. Our results also showed that SV40 T antigen positive cells were observed in the OSE (black arrows) of *TgK19GT*$_{121}$ mice and EOC (black arrows) of *Pten*$^{d/d}$ *Trp53*$^{d/d}$ *TgK19GT*$_{121}$ and *Pten*$^{d/d}$ *Trp53*$^{d/d}$ *Cdh1*$^{d/d}$ *TgK19GT*$_{121}$ mice (Figure 1E).

Impact of conditional inactivation of TRP53, PTEN, CDH1, and RB1 in the ovary

Nine different genotypes of mice (control, *Pten*$^{d/d}$, *Trp53*$^{d/d}$, *Cdh1*$^{d/d}$, *TgK19GT*$_{121}$, *Pten*$^{d/d}$ *Trp53*$^{d/d}$, *Pten*$^{d/d}$ *Trp53*$^{d/d}$ *Cdh1*$^{d/d}$, *Pten*$^{d/d}$ *Trp53*$^{d/d}$ *TgK19GT*$_{121}$, and *Pten*$^{d/d}$ *Trp53*$^{d/d}$ *Cdh1*$^{d/d}$ *TgK19GT*$_{121}$) were generated (n = 4–13 at each time point). Reproductive tract gross morphology was assessed at 6 month, *Pten*$^{d/d}$, *Trp53*$^{d/d}$, *Cdh1*$^{d/d}$, *TgK19GT*$_{121}$, *Pten*$^{d/d}$ *Trp53*$^{d/d}$, and *Pten*$^{d/d}$ *Trp53*$^{d/d}$ *Cdh1*$^{d/d}$ mice appeared to have normal ovaries based on the gross morphology of ovaries (Figure 2A and B). Histological analysis indicates that *Pten*$^{d/d}$ *Trp53*$^{d/d}$ *Cdh1*$^{d/d}$ mice did not show abnormal cancerous ovaries (Supplementary Figure S1), but an enlarged uterus (Figure 2B, arrow) was commonly (6 of 8 mice) observed in these mice at 6 months. Cre recombinase in *Amhr2*$^{Cre/+}$ mice is active in the uterine stroma and myometrium [26], potentially eliciting this abnormal morphology, but our focus was to characterize the role of these genes in OvCa. Because normal ovarian histology in *Pten*$^{d/d}$ mice has been reported [26] and mice with a double ablation of *Pten*$^{d/d}$ *Trp53*$^{d/d}$ possess ovaries with normal gross morphology (Figure 2A) and histology at 6 months (Supplementary Figure S1), *Trp53*$^{d/d}$, *Pten*$^{d/d}$, and *Pten*$^{d/d}$ *Trp53*$^{d/d}$ mice were removed from further analysis. *Pten*$^{d/d}$ *Trp53*$^{d/d}$ *TgK19GT*$_{121}$ and *Pten*$^{d/d}$ *Trp53*$^{d/d}$ *Cdh1*$^{d/d}$ *TgK19GT*$_{121}$ mice (n = 4–13, Table 1) exhibited enlarged ovarian tumors starting at 3 months (Figure 2B). *Pten*$^{d/d}$ *Trp53*$^{d/d}$ *TgK19GT*$_{121}$ mice (2 of 6 mice) and *Pten*$^{d/d}$ *Trp53*$^{d/d}$ *Cdh1*$^{d/d}$ *TgK19GT*$_{121}$ mice (8 of 13 mice) also showed abnormally enlarged uteri at 6 months (Supplementary Figure S2 and Table 1). Those putative uterine tumors were largely necrotic and contained large amount of putrid fluid. Ascites fluid accumulation and extensive peritoneal carcinomatosis with clusters of tumor nodules (black arrows, Figure 3A) and primary ovarian tumors (white arrows, Figure 3A) were observed in one *Pten*$^{d/d}$ *Trp53*$^{d/d}$ *TgK19GT*$_{121}$ mouse at 4 months (Figure 3 and Table 1). Metastatic tumors were detected in *Pten*$^{d/d}$ *Trp53*$^{d/d}$ *Cdh1*$^{d/d}$ *TgK19GT*$_{121}$ mice at 4 months (2 of 5 mice) and 6 months (5 of 13 mice) (Figure 3A and Table 1).

Kaplan–Meier analysis revealed that survival rates of *Pten*$^{d/d}$ *Trp53*$^{d/d}$ *TgK19GT*$_{121}$ and *Pten*$^{d/d}$ *Trp53*$^{d/d}$ *Cdh1*$^{d/d}$ *TgK19GT*$_{121}$ mice were significantly reduced ($P < 0.0001$, Figure 3B). While *Pten*$^{d/d}$ *Trp53*$^{d/d}$ *TgK19GT*$_{121}$ and *Pten*$^{d/d}$ *Trp53*$^{d/d}$ *Cdh1*$^{d/d}$ *TgK19GT*$_{121}$ mice exhibited a median survival of 5.3 months, 71.8% of *Pten*$^{d/d}$ *Trp53*$^{d/d}$ *TgK19GT*$_{121}$ and 100% of *Pten*$^{d/d}$ *Trp53*$^{d/d}$ *Cdh1*$^{d/d}$ *TgK19GT*$_{121}$ mice died or reached our tumor burden euthanasia criteria by 6.5 months. We observed that more mice with *Pten*$^{d/d}$ *Trp53*$^{d/d}$ *TgK19GT*$_{121}$ compared to mice with *Pten*$^{d/d}$ *Trp53*$^{d/d}$ *Cdh1*$^{d/d}$ *TgK19GT*$_{121}$ died prior to 4.5 months (black arrow in Figure 3B). Some *Pten*$^{d/d}$ *Trp53*$^{d/d}$ *TgK19GT*$_{121}$ mice were still alive at 6–6.5 months, whereas no *Pten*$^{d/d}$ *Trp53*$^{d/d}$ *Cdh1*$^{d/d}$ *TgK19GT*$_{121}$ mice survived to 6.5 months. The uterine tumor burden observed in a few *Pten*$^{d/d}$ *Trp53*$^{d/d}$ *Cdh1*$^{d/d}$ mice led to death/euthanasia between 4 and 6.5 months (Figure 3B), whereas median survival was undefined by Kaplan–Meier analysis. Control, *Cdh1*$^{d/d}$, *TgK19GT*$_{121}$, and *Pten*$^{d/d}$ *Trp53*$^{d/d}$ mice appeared healthy until at least 6.5 months.

Histopathology of OvCa in Pten$^{d/d}$, Trp53$^{d/d}$ TgK19GT$_{121}$, and Pten$^{d/d}$ Trp53$^{d/d}$ Cdh1$^{d/d}$ TgK19GT$_{121}$ mice

Histopathological examination demonstrated that single ablation of *Pten*, *Trp53*, or *Cdh1*, and inactivation of RB1, double ablation of *Pten* and *Trp53*, as well as triple ablation of *Pten*, *Trp53*, and *Cdh1* in the ovary by 6 months did not show in any abnormalities (Supplementary Figure S1). In contrast, *Pten*$^{d/d}$ *Trp53*$^{d/d}$ *TgK19GT*$_{121}$ and *Pten*$^{d/d}$ *Trp53*$^{d/d}$ *Cdh1*$^{d/d}$ *TgK19GT*$_{121}$ mice developed similar features of EOC (Figure 4). However, initiation of EOC occurs earlier in *Pten*$^{d/d}$ *Trp53*$^{d/d}$ *TgK19GT*$_{121}$ mice (Figure 4a and Table 1). *Pten*$^{d/d}$ *Trp53*$^{d/d}$ *TgK19GT*$_{121}$ mice developed epithelial hyperplasia (5 of 7 mice) and low-grade serous micropapillary carcinomas (4 of 7 mice) that originated from the OSE at 1 months (Figure 4a and Table 1). The first signs of epithelial hyperplasia (3 of 9 mice) and micropapillary features (4 of 9 mice) in the OSE of *Pten*$^{d/d}$ *Trp53*$^{d/d}$ *Cdh1*$^{d/d}$ *TgK19GT*$_{121}$ mice were observed at 2 months (Figure 4f and Table 1). No *Pten*$^{d/d}$ *Trp53*$^{d/d}$ *Cdh1*$^{d/d}$ *TgK19GT*$_{121}$ mice (0 of 8 mice) showed abnormal OSE at 1 months (Figure 4e and Table 1). However, around 3–4 months, both *Pten*$^{d/d}$ *Trp53*$^{d/d}$ *TgK19GT*$_{121}$ and *Pten*$^{d/d}$ *Trp53*$^{d/d}$ *Cdh1*$^{d/d}$ *TgK19GT*$_{121}$ mice exhibited invasion of serous carcinomas into the ovary with papillary and some HGSC features (Figure 4c and g and Table 1). When some of these mice started dying at ~4 months in both genotypes, we observed that EOC had already invaded into the entire ovary and the peritoneal cavity. The features of HGSC were first observed at 3 months in *Pten*$^{d/d}$ *Trp53*$^{d/d}$ *TgK19GT*$_{121}$ mice and at 4 months in *Pten*$^{d/d}$ *Trp53*$^{d/d}$ *Cdh1*$^{d/d}$ *TgK19GT*$_{121}$ mice (Table 1). At 6 months (Figure 4d and h and Table 1), *Pten*$^{d/d}$ *Trp53*$^{d/d}$ *Cdh1*$^{d/d}$ *TgK19GT*$_{121}$ mice showed increased features of serous papillary carcinoma (9 of 13 mice) and HGSC (5 of 13 mice), as well as ascites fluid accumulation (5 of 13 mice), and peritoneal carcinomatosis (5 of 13 mice). In contrast, *Pten*$^{d/d}$ *Trp53*$^{d/d}$ *TgK19GT*$_{121}$ mice exhibited less HGSC (1 of 6 mice), but showed some granulosa cell tumors (2 of 6 mice).

As shown in Table 1, both genotypes of mice developed heterogeneous OvCa with papillary, HGSC, granulosa cell tumors, and/or necrotic tumors, whereas other types of EOC such as endometrioid,

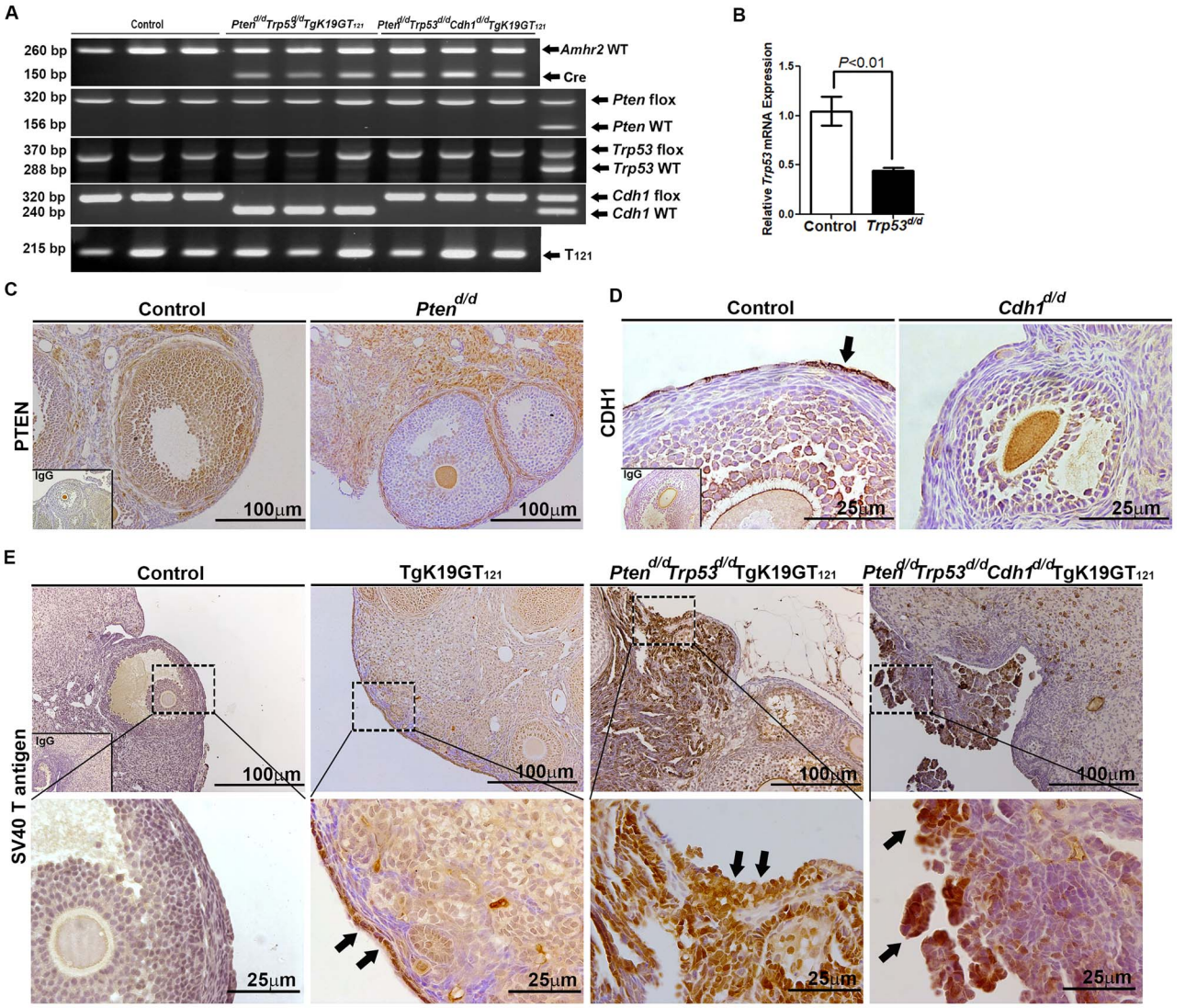

Figure 1. Analysis of conditional ablation/inactivation of *Pten, Trp53, Cdh1,* and *Rb1* induced by $Amhr2^{Cre/+}$ mice in mouse ovary. (A) Genotyping PCR of tail DNA to detect the $Amhr2^{Cre/+}$ transgene (three representative mice per each genotype and heterozygous, f/+). (B) QPCR analysis of *Trp53* normalized to *Rpl19* in the ovary of control and $Trp53^{d/d}$ mice. Immunolocalization of (C) PTEN in the ovary of control and $Pten^{d/d}$ mice; (D) CDH1 in the ovary of control and $Cdh1^{d/d}$ mice; and (E) SV40 T antigen in the ovary of control, $TgK19GT_{121}$, $Pten^{d/d}$ $Trp53^{d/d}$ $TgK19GT_{121}$, and $Pten^{d/d}$ $Trp53^{d/d}$ $Cdh1^{d/d}$ $TgK19GT_{121}$ mice. Black arrows show positive immunostaining.

clear cell, and mucinous carcinomas were not observed. In contrast, serous papillary carcinomas were enlarged during the progression of OvCa in both genotypes. While there was some variability within animals of each group, several histopathological OvCa features were commonly identified in both genotypes including EOC hyperplasia (Figure 5a, arrow), progression of micropapillary and papillary carcinomas originating from the OSE (Figure 5b and c), papillary structure with slit-like spaces (Figure 5d), and papillary architecture with cytosolic atypia (Figure 5e). In addition, HGSC was also observed (Figure 5f), especially in the later stages of OvCa progression, characterized by nuclear atypia (Figure 5g, arrows), apoptotic cells (Figure 5h, arrow), abnormal mitosis (Figure 5i, arrows), and cell clumps (Figure 5j, arrow). We also observed cribriform architecture (Figure 5k), granulosa cell tumors (Figure 5l), papillary architecture with necrosis (Figure 5m), necrotic tumors (Figure 5n), papillary carcinoma with cystic features (Figure 5o), and dissemination of tumors into the peritoneal cavity (Figure 5p). However, oviducts of mice from both genotypes showed normal histology (Figure 5q).

Strong staining of Ki67 positive cells, as a marker of cell proliferation, was observed within hyperplastic OSE (black arrows) at 2 months and OvCa tumors at 2–3 months in $Pten^{d/d}$ $Trp53^{d/d}$ $Cdh1^{d/d}$ $TgK19GT_{121}$ mice, suggesting abnormal proliferation was present (Figure 6A). In contrast, control OSE lacked Ki67 staining, normal granulosa cells within growing follicles serve as a positive control for staining in healthy follicles. Those hyperplastic OSE (black arrows) at 2 months and OvCa at 2–3 months showed strong expression of KRT14, a marker of epithelial cells, and WT1, a marker of cancer cells in EOC (Figure 6A). Note: WT1 is known to be detectable in normal granulosa cells [29, 30]. PAX8, a marker of oviductal epithelial cells, was not detected within OvCa tumors, but was not altered in oviductal cells of ovarian sections of mice with EOC (Figure 6B). Similar staining was observed in $Pten^{d/d}$ $Trp53^{d/d}$ $TgK19GT_{121}$ (data not shown). CDH1 was positive in OSE in control mice (white

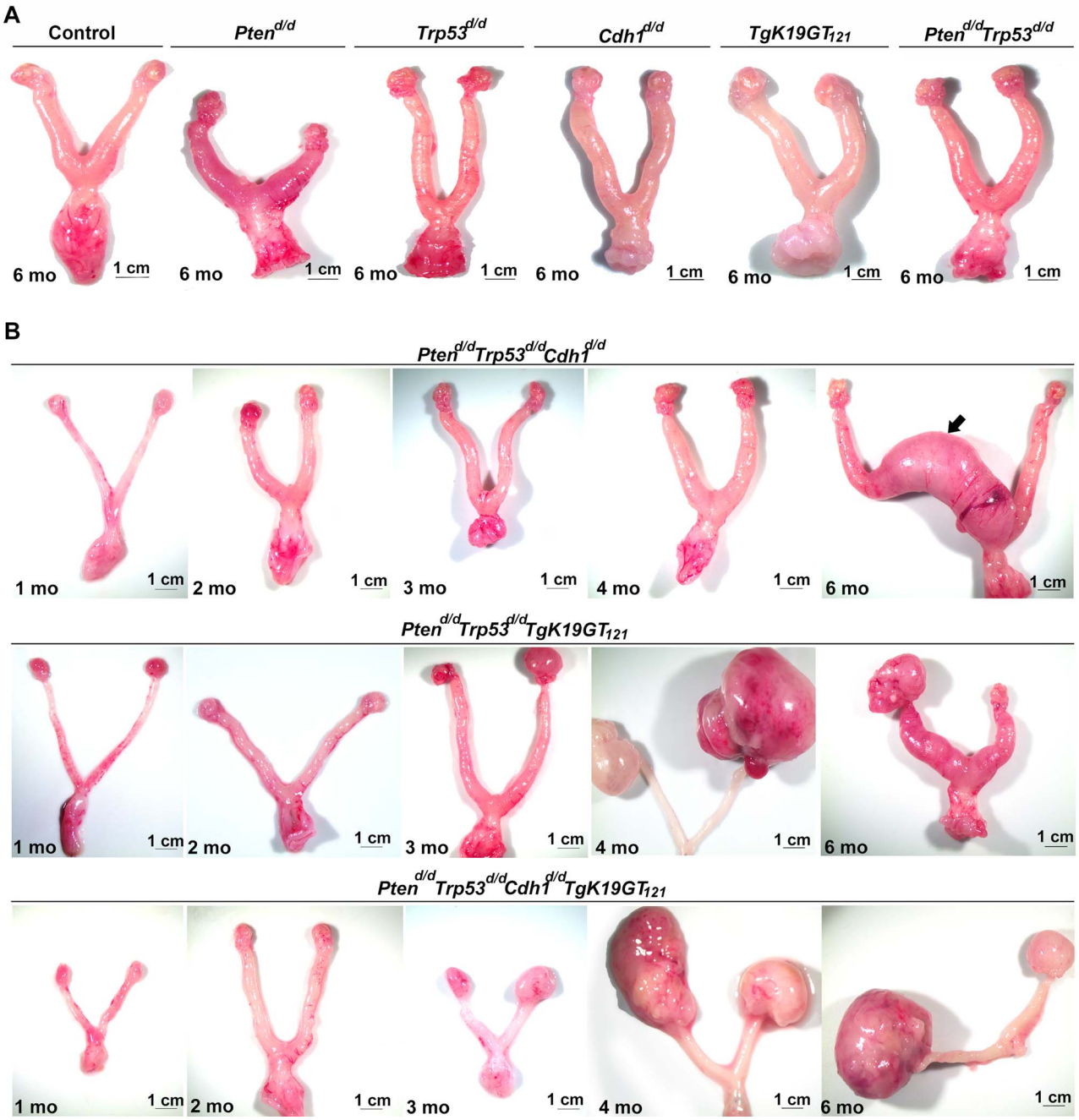

Figure 2. Gross morphology of the female reproductive tract in (A) control, *Pten*$^{d/d}$, *Trp53*$^{d/d}$, *Cdh1*$^{d/d}$, *TgK19GT*$_{121}$, and *Pten*$^{d/d}$ *Trp53*$^{d/d}$ at 6 months of age; and (B) *Pten*$^{d/d}$ *Trp53*$^{d/d}$ *Cdh1*$^{d/d}$, *Pten*$^{d/d}$ *Trp53*$^{d/d}$ *TgK19GT*$_{121}$, and *Pten*$^{d/d}$ *Trp53*$^{d/d}$ *Cdh1*$^{d/d}$ *TgK19GT*$_{121}$ mice at 1–6 months of age. Arrow indicates uterine enlargement observed in 75% of *Pten*$^{d/d}$ *Trp53*$^{d/d}$ *Cdh1*$^{d/d}$ mice at 6 months.

arrow) and EOC in *Pten*$^{d/d}$ *Trp53*$^{d/d}$ *TgK19GT*$_{121}$ mice, but not present in *Pten*$^{d/d}$ *Trp53*$^{d/d}$ *Cdh1*$^{d/d}$ *TgK19GT*$_{121}$ mice (Figure 6C). Note: CDH1 is positive in oocytes, and granulosa cells show some background fluorescence (see IgG control). Disseminated tumors retrieved from the peritoneal cavity displayed strong Ki67, KRT14, and WT1 expression throughout the tissue section (Figure 6D).

Discussion

The Cancer Genome Atlas (TCGA) dataset indicates that HGSC harbor *TP53* mutations in at least 96% of tumors [5]. Deregulation of the RB1 and PI3K pathways has been reported in 67 and 45% of HGSC, respectively [5]. While homozygous *PTEN* mutations are found in 7% of HGSC [5], total or partial loss of PTEN protein was reported in 15 or 50% of HGSC, respectively [31], implying that loss of PTEN function could be an induction of aberrant AKT activation in HGSC. Loss of CDH1 function has been implicated in the progression and metastasis of numerous malignancies [17–19]. Disruption of epithelial cells routinely occurs in the OSE during ovulation. Damaged OSE can result in the formation of a cyst with an epithelial lining inside and can be the origin of EOC [3]. In fact, the increased number of ovulations is considered as one of the risk factors of EOC

Table 1. Characteristics of *Pten*$^{d/d}$ *Trp53*$^{d/d}$ *TgK19GT*$_{121}$ and *Pten*$^{d/d}$ *Trp53*$^{d/d}$ *Cdh1*$^{d/d}$ *TgK19GT*$_{121}$ mice.

Genotype	Phenotype	Age				
		1 month	2 months	3 months	4 months	6 months
Pten$^{d/d}$ *Trp53*$^{d/d}$ *TgK19GT*$_{121}$	OSE hyperplasia	71.4% (5/7)	11.1% (1/9)	0%	0%	50.0% (3/6)
	Serous papillary carcinomas	57.1% (4/7)	44.4% (4/9)	71.4% (5/7)	100.0% (5/5)	50.0% (3/6)
	HGSC	0%	0%	14.3% (1/7)	60.0% (3/5)	16.7% (1/6)
	Peritoneal metastasis	0%	0%	0%	60.0% (3/5)	0%
	Ascites fluid accumulation	0%	0%	0%	20.0% (1/5)	0%
	Granulosa cell tumors	0%	11.1% (1/9)	0%	0%	33.3% (2/6)
	Necrotic tumors	0%	0%	14.3% (1/7)	0%	0%
	Uterine tumors	0%	0%	0%	0%	16.7% (2/6)
Pten $^{d/d}$ *Trp53* $^{d/d}$ *Cdh1* $^{d/d}$ *TgK19GT* $_{121}$	OSE hyperplasia	0% (0/8)	30.0% (3/9)	25.0% (1/4)	0%	0%
	Serous papillary carcinomas	0%	44.4% (4/9)	75.0% (3/4)	80.0% (4/5)	69.2% (9/13)
	HGSC	0%	0%	0%	20.0% (1/5)	38.5% (5/13)
	Peritoneal metastasis	0%	0%	0%	40.0% (2/5)	38.5% (5/13)
	Ascites fluid accumulation	0%	0%	0%	40.0% (2/5)	38.5% (5/13)
	Granulosa cell tumors	0%	0%	0%	0%	0%
	Necrotic tumors	0%	0%	0%	20.0% (1/5)	0%
	Uterine tumors	0%	0%	0%	0%	61.5% (8/13)

[16]. Owing to those clinical features of OvCa, we have generated and characterized a mouse model in which TRP53, PTEN, RB1, and/or CDH1 are conditionally inactivated using *Amhr2*$^{cre/+}$. Based on the specificity of RB1 inactivation in KRT19-expressing cells [22] and the results of initial epithelial hyperplasia in the OSE, the present study indicates that EOC originates from the OSE. Although histopathological analysis revealed that most tumors developed type I low-grade OvCa with the features of serous papillary carcinomas, some of the tumors became HGSCs exhibiting nuclear atypia and peritoneal metastasis. It has been reported that the OSE can develop into serous papillary adenocarcinomas, when *Amhr2*$^{cre/+}$ mice are used to mutate *Pten* and express *Kras*^{G12D} [9]. With an addition of *Trp53*^{R172H} mutant expression to disruption of *Pten* gene and *Kras*^{G12D}, OSE forms mucinous with serous features of carcinomas [11]. *Pten* deletion and *Trp53*^{R172H} mutation are also able to develop HGSC [10]. Adenovirus-Cre-mediated ablation of *Trp53* and *Rb1* [32] in the OSE induces poorly differentiated carcinomas. Inactivation of TRP53, RB1, and BRCA1/2 in the OSE leads to the development of ovarian tumors with HGSC phenotype [23]. These results suggest that altered combinations of TRP53, RB1, and PTEN functions in the OSE are most likely critical to induce low- and high-grade features of EOC.

In our model, inactivation of TRP53, PTEN, and RB1 with or without CDH1 ablation showed similar pathogenesis including enlarged focal areas of papillary differentiation as shown in Figure 4. On the other hand, *Pten*$^{d/d}$ *Trp53*$^{d/d}$ *TgK19GT*$_{121}$ mice initiated OSE hyperplasia and micropapillary differentiation at the age of 1 month (Figure 4a). Interestingly, the initiation of EOC in *Pten*$^{d/d}$ *Trp53*$^{d/d}$ *TgK19GT*$_{121}$ mice started earlier than that in *Pten*$^{d/d}$ *Trp53*$^{d/d}$ *Cdh1*$^{d/d}$ *TgK19GT*$_{121}$ mice (Figure 4a and e). Although we do not have a direct answer to address this observation, disruption of epithelial cells by loss of CDH1 in the OSE might lead to insufficient epithelial ablation/inactivation of TRP53, PTEN, and RB1, slowing down the progression of carcinogenesis. One possibility is that the loss of CDH1 leads to sloughing and death of abnormal epithelial cells that might otherwise lead to cancer. In fact, survival rate of *Pten*$^{d/d}$ *Trp53*$^{d/d}$ *TgK19GT*$_{121}$ mice dropped 50% around 4 months, whereas ~75% of *Pten*$^{d/d}$ *Trp53*$^{d/d}$ *Cdh1*$^{d/d}$ *TgK19GT*$_{121}$ mice survived until 5 months. However, a few more *Pten*$^{d/d}$ *Trp53*$^{d/d}$ *Cdh1*$^{d/d}$ *TgK19GT*$_{121}$ mice developed HGSC, serous papillary carcinomas, and/or metastatic tumors at 6 months of age, and all mice died by 6.5 months. We observed that some of *Pten*$^{d/d}$ *Trp53*$^{d/d}$ *TgK19GT*$_{121}$ mice survived past the time-point of 4 months, and those mice showed less invasive and aggressive features. Indeed, we did not find any signs of metastasis in *Pten*$^{d/d}$ *Trp53*$^{d/d}$ *TgK19GT*$_{121}$ mice that survived at 6 months. Thus, TRP53, PTEN, and RB1 inactivation is enough to initiate and progress early tumor development, whereas loss of CDH1 eventually accelerates invasive and metastatic progression of tumorigenesis in OvCa. On the other hand, HGSC was observed in older mice at 3–6 months for *Pten*$^{d/d}$ *Trp53*$^{d/d}$ *TgK19GT*$_{121}$ mice, or 4–6 months for *Pten*$^{d/d}$ *Trp53*$^{d/d}$ *Cdh1*$^{d/d}$ *TgK19GT*$_{121}$ mice, whereas low-grade serous papillary carcinomas have been observed from the early EOC development. These results let us speculate that HGSC could be differentiated from serous papillary carcinomas. However, the initiation and development of HGSC might be separately considered differentiation from other types of EOC, because HGSC has been detected in early stages of OvCa in clinical studies [3].

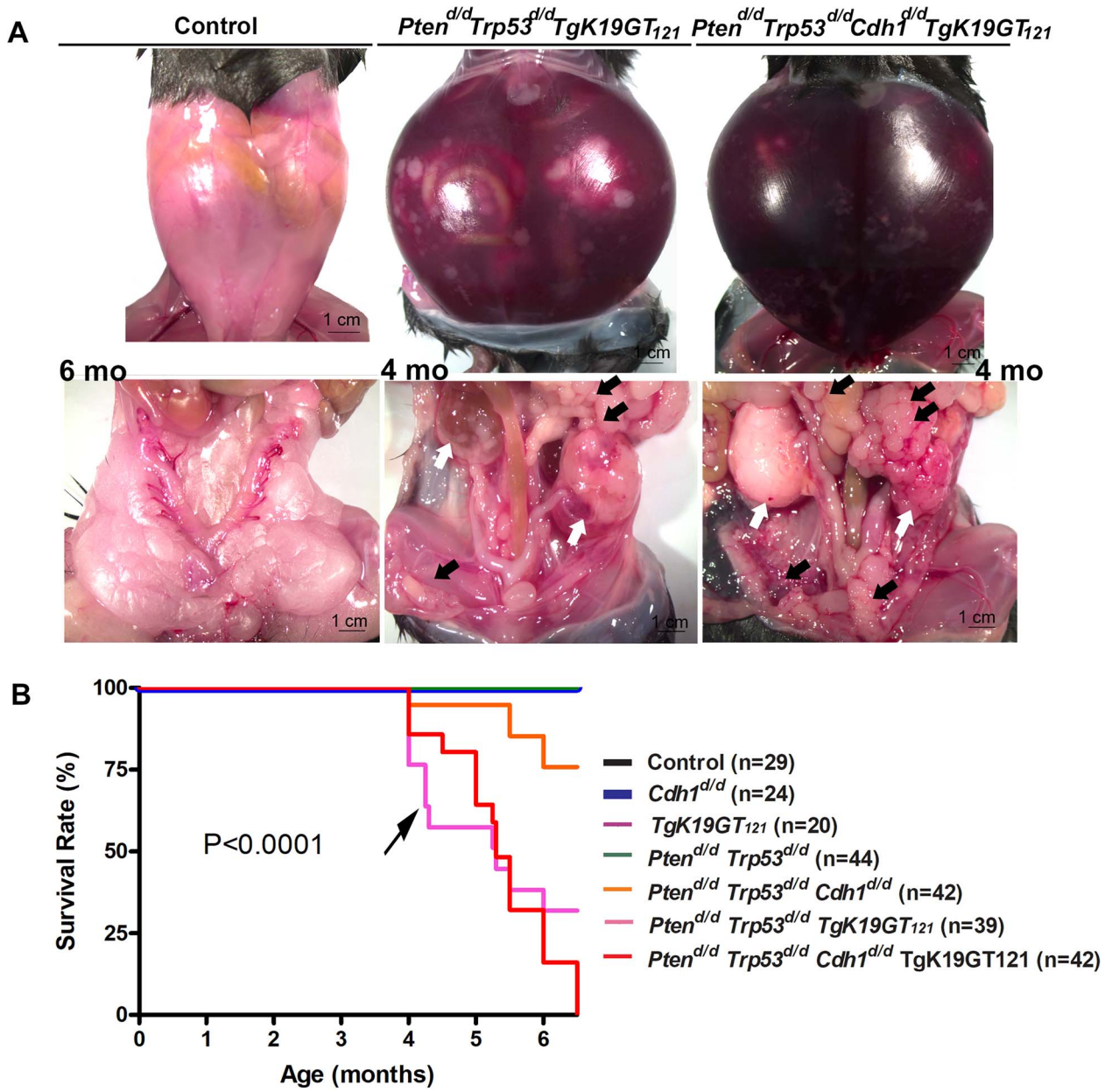

Figure 3. (A) Ascites fluid accumulation and peritoneal carcinomatosis tumors were observed in $Pten^{d/d}$ $Trp53^{d/d}$ $TgK19GT_{121}$ and $Pten^{d/d}$ $Trp53^{d/d}$ $Cdh1^{d/d}$ $TgK19GT_{121}$ mice. White arrows show primary ovarian tumors and black arrows show extensive peritoneal carcinomatosis with clusters of tumor nodules. (B) Overall survival rate for control, $Cdh1^{d/d}$, $TgK19GT_{121}$, $Pten^{d/d}$ $Trp53^{d/d}$, $Pten^{d/d}$ $Trp53^{d/d}$ $Cdh1^{d/d}$, $Pten^{d/d}$ $Trp53^{d/d}$ $TgK19GT_{121}$, and $Pten^{d/d}$ $Trp53^{d/d}$ $Cdh1^{d/d}$ $TgK19GT_{121}$ mice was determined by Kaplan–Meier analysis ($P < 0.0001$). All mice were monitored for any sign of sickness or discomfort. When present, those mice were euthanized, and the day of sacrifice was recorded. Black arrow shows that more mice with $Pten^{d/d}$ $Trp53^{d/d}$ $TgK19GT_{121}$ died by 4.5 months compared to mice with $Pten^{d/d}$ $Trp53^{d/d}$ $Cdh1^{d/d}$ $TgK19GT_{121}$.

We have occasionally observed granulosa cell tumors in $Pten^{d/d}$ $Trp53^{d/d}$ $TgK19GT_{121}$ mice. This observation is surprising, because RB1 inactivation via Cre-dependent induction of the *Krt19* promoter in $Pten^{d/d}$ $Trp53^{d/d}$ $TgK19GT_{121}$ should be limited only to OSE. Thus, these animals would possess granulosa-specific deletion for only TRP53 and PTEN. However, $Pten^{d/d}$ $Trp53^{d/d}$ mice did not show any abnormal histopathology in the ovary, indicating that inactivation of RB1 in the OSE and loss of *Trp53* and *Pten* either in OSE or granulosa cells somehow could associate to induce granulosa cell tumors.

Based on the results of PAX8 expression, our model did not induce any tumors derived from the stroma of the oviduct where *Amhr2-Cre* recombinase is active. Since inactivation of RB1 and CDH1 is limited to epithelial cells, this result indicates that *Amhr2-Cre*-driven ablation of TRP53 and PTEN in the stroma of the oviduct is not able to induce tumorigenesis. The use of *Pax8* or *Ovgp1* promoters to express Cre recombinase is able to target in oviductal epithelial cells of oviduct [12–15]. Targeting *Brca1/2*, $Trp53^{R172H}$, and *Pten* genes using $Pax8^{cre}$ induces HGSC originated from the oviduct [12]. *Brca1*, *Trp53*, *Rb1*, *Nf1*, and/or *Pten* defects using

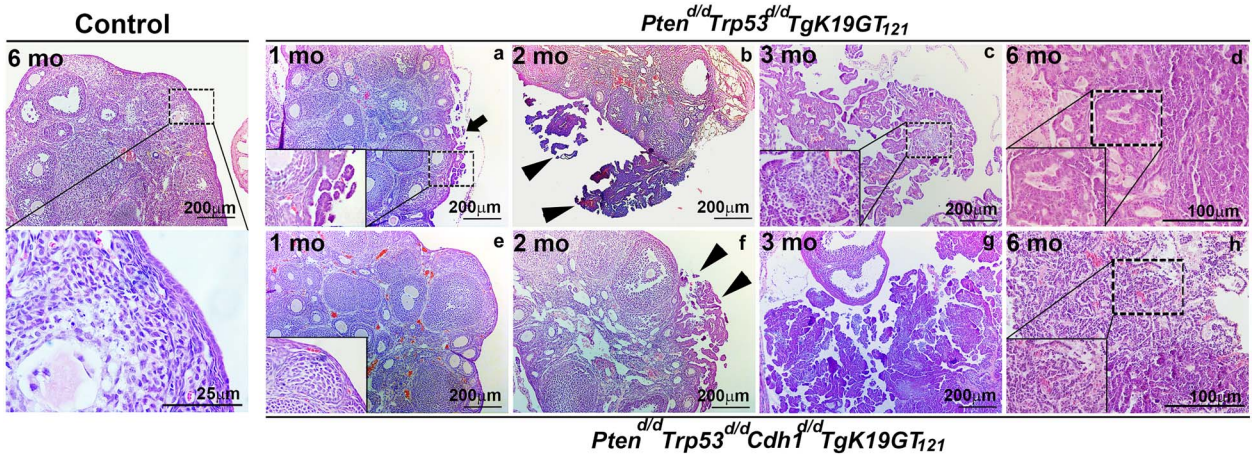

Figure 4. Ovarian histopathology of control, *Pten*$^{d/d}$ *Trp53*$^{d/d}$ *TgK19GT*$_{121}$, and *Pten*$^{d/d}$ *Trp53*$^{d/d}$ *Cdh1*$^{d/d}$ *TgK19GT*$_{121}$ mice at 1–6 months of age (a–h). Tissues were stained using H&E. Black arrow indicates ovarian surface epithelial hyperplasia and arrowheads show serous micropapillary carcinomas.

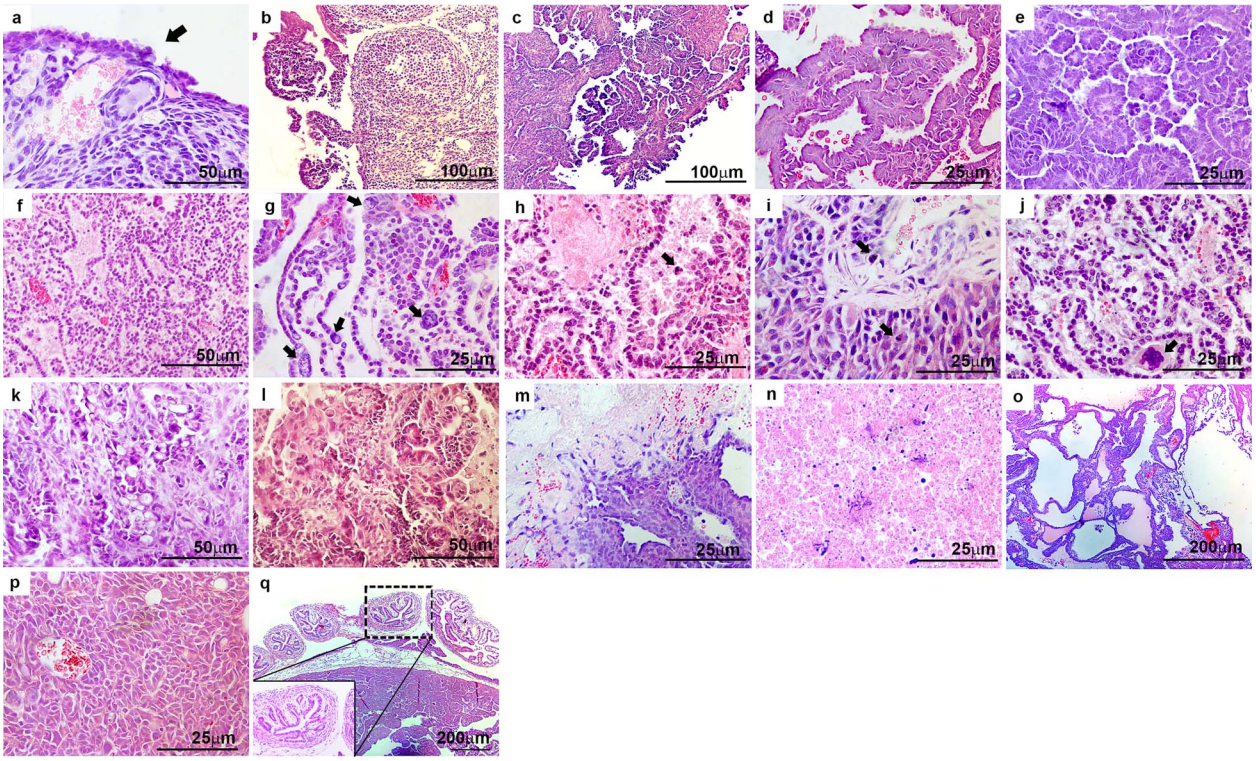

Figure 5. *Pten*$^{d/d}$ *Trp53*$^{d/d}$ *TgK19GT*$_{121}$ and *Pten*$^{d/d}$ *Trp53*$^{d/d}$ *Cdh1*$^{d/d}$ *TgK19GT*$_{121}$ mice possess many histopathological features of OvCa in common. Representative images are presented for: (a) epithelial hyperplasia (black arrow), (b, c) progression of micropapillary and papillary carcinomas, (d) papillary structure with slit-like spaces, (e) papillary architecture with cytosolic atypia, (f) high-grade serous carcinoma (HGSC), (g–j) representative features of HGSC with (g) nuclear atypia (black arrows), (h) apoptotic cells (black arrow), (i) abnormal mitosis (black arrows), (j) cell clumps (black arrow), (k) cribriform architecture, (l) granulosa cell tumor, (m) papillary architecture with necrosis, (n) necrotic tumor, (o) papillary with cystic features, (p) peritoneal metastatic tumor, and (q) normal oviduct.

Ovgp1-iCre-ER^{T2} result in serous tubal intraepithelial carcinomas and HGSC [14]. These results suggest that inactivation of genes in the epithelial cells of the oviduct is crucial to develop OvCa. On the other hand, we observed uterine tumor burden in some *Pten*$^{d/d}$ *Trp53*$^{d/d}$ *Cdh1*$^{d/d}$, *Pten*$^{d/d}$ *Trp53*$^{d/d}$ *TgK19GT*$_{121}$, or *Pten*$^{d/d}$ *Trp53*$^{d/d}$ *Cdh1*$^{d/d}$ *TgK19GT*$_{121}$ mice at 6 months of age. Within the uterus, AMHR2 expression is limited only to the stroma and myometrium [26]. Thus, inactivation of TRP53 and PTEN is only likely to be induced in the uterus. However, *Pten*$^{d/d}$ *Trp53*$^{d/d}$ mice did not show any abnormal uterine morphology. It has been reported that loss of PTEN by *Amhr2*$^{cre/+}$ mice fails to induce endometrial cancer, but generates abnormal myometrial adipogenesis [26]. Although the reasons for the development of necrotic uterine tumor burden observed in *Pten*$^{d/d}$ *Trp53*$^{d/d}$ *Cdh1*$^{d/d}$, *Pten*$^{d/d}$ *Trp53*$^{d/d}$ *TgK19GT*$_{121}$,

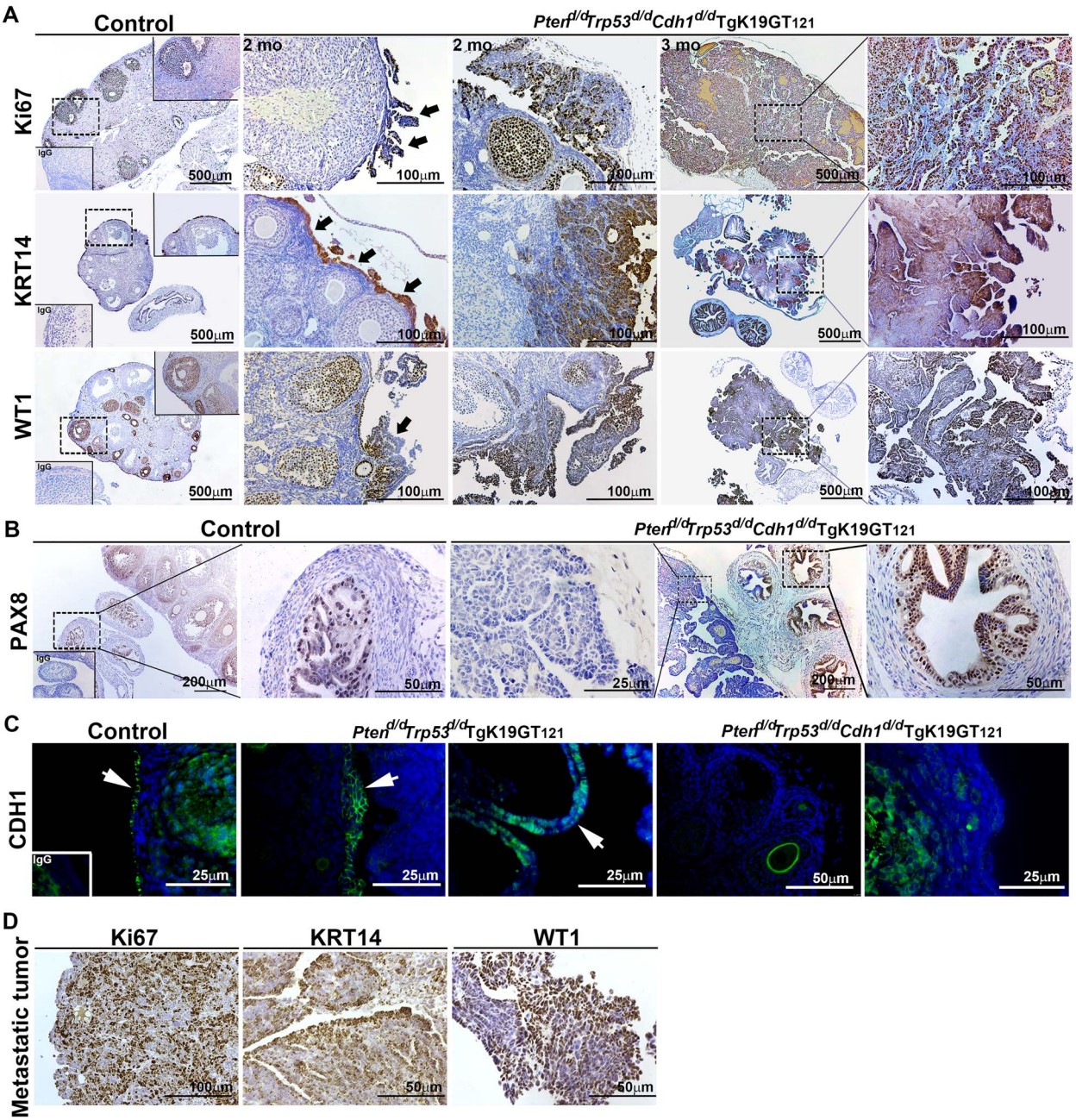

Figure 6. Immunohistochemical analysis of (A) Ki67 as a marker of cell proliferation, KRT14 as a marker of epithelial cells, and WT1 as a marker of cancer cells (black arrows show hyperplastic OSE at 2 months), (B) PAX8 as a marker of oviductal epithelial cells in *Pten*$^{d/d}$ *Trp53*$^{d/d}$ *Cdh1*$^{d/d}$ *TgK19GT*$_{121}$ mice. Similar staining was observed in *Pten*$^{d/d}$ *Trp53*$^{d/d}$ *TgK19GT*$_{121}$ (data not shown). (C) CDH1 (white arrows show CDH1 positive cells) in control, *Pten*$^{d/d}$ *Trp53*$^{d/d}$ *TgK19GT*$_{121}$, and *Pten*$^{d/d}$ *Trp53*$^{d/d}$ *Cdh1*$^{d/d}$ *TgK19GT*$_{121}$ mice. (D) Immunohistochemical analysis of Ki67, KRT14, and WT1 in metastatic tumors.

or *Pten*$^{d/d}$ *Trp53*$^{d/d}$ *Cdh1*$^{d/d}$ *TgK19GT*$_{121}$ mice are still unclear, those tumors might be endometrial adenosarcoma, which might warrant further investigation in the future to determine the suitability of this model for uterine cancer studies.

Collectively, the results of the present study suggest that the impact of inactivation of TRP53, PTEN, and RB1 in the OSE causes development of EOC with low-grade serous papillary carcinomas and HGSC. Ablation of CDH1 further accelerates the development of aggressive metastatic tumors at later stages. In contrast, EOC from the OSE did not initiate HGSC at early stage of OvCa development.

Supplementary data

Supplementary data are available at *BIOLRE* online.

Acknowledgments

We thank Dr. Richard R. Behringer at The University of Texas, MD Anderson Cancer Center for providing us *Amhr2*$^{cre/+}$ mice.

Conflict of Interest

The authors have nothing to disclose.

References

1. Siegel RL, Miller KD, Jemal A. Cancer statistics, 2019. *CA Cancer J Clin* 2019; **69**:7–34.
2. Cho KR, Shih Ie M. Ovarian cancer. *Annu Rev Pathol* 2009; **4**:287–313.
3. Kim J, Park EY, Kim O, Schilder JM, Coffey DM, Cho CH, Bast RC Jr. Cell origins of high-grade serous ovarian cancer. *Cancers (Basel)* 2018; **10**.
4. Kurman RJ, Shih Ie M. Pathogenesis of ovarian cancer: lessons from morphology and molecular biology and their clinical implications. *Int J Gynecol Pathol* 2008; **27**:151–160.
5. Cancer Genome Atlas Research. Integrated genomic analyses of ovarian carcinoma. *Nature* 2011; **474**:609–615.
6. Bobbs AS, Cole JM, Cowden Dahl KD. Emerging and evolving ovarian cancer animal models. *Cancer Growth Metastasis* 2015; **8**:29–36.
7. Lengyel E, Burdette JE, Kenny HA, Matei D, Pilrose J, Haluska P, Nephew KP, Hales DB, Stack MS. Epithelial ovarian cancer experimental models. *Oncogene* 2014; **33**:3619–3633.
8. Morin PJ, Weeraratna AT. Genetically-defined ovarian cancer mouse models. *J Pathol* 2016; **238**:180–184.
9. Fan HY, Liu Z, Paquet M, Wang J, Lydon JP, DeMayo FJ, Richards JS. Cell type-specific targeted mutations of Kras and Pten document proliferation arrest in granulosa cells versus oncogenic insult to ovarian surface epithelial cells. *Cancer Res* 2009; **69**:6463–6472.
10. Kim J, Coffey DM, Ma L, Matzuk MM. The ovary is an alternative site of origin for high-grade serous ovarian cancer in mice. *Endocrinology* 2015; **156**:1975–1981.
11. Ren YA, Mullany LK, Liu Z, Herron AJ, Wong KK, Richards JS. Mutant p53 promotes epithelial ovarian cancer by regulating tumor differentiation, metastasis, and responsiveness to steroid hormones. *Cancer Res* 2016; **76**:2206–2218.
12. Perets R, Wyant GA, Muto KW, Bijron JG, Poole BB, Chin KT, Chen JY, Ohman AW, Stepule CD, Kwak S, Karst AM, Hirsch MS et al. Transformation of the fallopian tube secretory epithelium leads to high-grade serous ovarian cancer in Brca;Tp53;Pten models. *Cancer Cell* 2013; **24**:751–765.
13. Russo A, Czarnecki AA, Dean M, Modi DA, Lantvit DD, Hardy L, Baligod S, Davis DA, Wei JJ, Burdette JE. PTEN loss in the fallopian tube induces hyperplasia and ovarian tumor formation. *Oncogene* 2018; **37**:1976–1990.
14. Zhai Y, Wu R, Kuick R, Sessine MS, Schulman S, Green M, Fearon ER, Cho KR. High-grade serous carcinomas arise in the mouse oviduct via defects linked to the human disease. *J Pathol* 2017; **243**:16–25.
15. Wu R, Zhai Y, Kuick R, Karnezis AN, Garcia P, Naseem A, Hu TC, Fearon ER, Cho KR. Impact of oviductal versus ovarian epithelial cell of origin on ovarian endometrioid carcinoma phenotype in the mouse. *J Pathol* 2016; **240**:341–351.
16. Purdie DM, Bain CJ, Siskind V, Webb PM, Green AC. Ovulation and risk of epithelial ovarian cancer. *Int J Cancer* 2003; **104**:228–232.
17. Frixen UH, Behrens J, Sachs M, Eberle G, Voss B, Warda A, Lochner D, Birchmeier W. E-cadherin-mediated cell-cell adhesion prevents invasiveness of human carcinoma cells. *J Cell Biol* 1991; **113**:173–185.
18. Perl AK, Wilgenbus P, Dahl U, Semb H, Christofori G. A causal role for E-cadherin in the transition from adenoma to carcinoma. *Nature* 1998; **392**:190–193.
19. Vleminckx K, Vakaet L Jr, Mareel M, Fiers W, van Roy F. Genetic manipulation of E-cadherin expression by epithelial tumor cells reveals an invasion suppressor role. *Cell* 1991; **66**:107–119.
20. Burkholder T, Foltz C, Karlsson E, Linton CG, Smith JM. Health evaluation of experimental laboratory mice. *Curr Protoc Mouse Biol* 2012; **2**:145–165.
21. Jamin SP, Arango NA, Mishina Y, Hanks MC, Behringer RR. Requirement of Bmpr1a for Mullerian duct regression during male sexual development. *Nat Genet* 2002; **32**:408–410.
22. Song Y, Gilbert D, O'Sullivan TN, Yang C, Pan W, Fathalizadeh A, Lu L, Haines DC, Martin PL, Van Dyke T. Carcinoma initiation via RB tumor suppressor inactivation: a versatile approach to epithelial subtype-dependent cancer initiation in diverse tissues. *PLoS One* 2013; **8**: e80459.
23. Szabova L, Yin C, Bupp S, Guerin TM, Schlomer JJ, Householder DB, Baran ML, Yi M, Song Y, Sun W, McDunn JE, Martin PL et al. Perturbation of Rb, p53, and Brca1 or Brca2 cooperate in inducing metastatic serous epithelial ovarian cancer. *Cancer Res* 2012; **72**:4141–4153.
24. Cho KR. Ovarian cancer update: Lessons from morphology, molecules, and mice. *Arch Pathol Lab Med* 2009; **133**:1775–1781.
25. Hayashi K, Erikson DW, Tilford SA, Bany BM, Maclean JA 2nd, Rucker EB 3rd, Johnson GA, Spencer TE. Wnt genes in the mouse uterus: Potential regulation of implantation. *Biol Reprod* 2009; **80**:989–1000.
26. Daikoku T, Jackson L, Besnard V, Whitsett J, Ellenson LH, Dey SK. Cell-specific conditional deletion of Pten in the uterus results in differential phenotypes. *Gynecol Oncol* 2011; **122**:424–429.
27. Mullany LK, Fan HY, Liu Z, White LD, Marshall A, Gunaratne P, Anderson ML, Creighton CJ, Xin L, Deavers M, Wong KK, Richards JS. Molecular and functional characteristics of ovarian surface epithelial cells transformed by KrasG12D and loss of Pten in a mouse model in vivo. *Oncogene* 2011; **30**:3522–3536.
28. Richards JS, Fan HY, Liu Z, Tsoi M, Lague MN, Boyer A, Boerboom D. Either Kras activation or Pten loss similarly enhance the dominant-stable CTNNB1-induced genetic program to promote granulosa cell tumor development in the ovary and testis. *Oncogene* 2012; **31**:1504–1520.
29. Chen M, Zhang L, Cui X, Lin X, Li Y, Wang Y, Wang Y, Qin Y, Chen D, Han C, Zhou B, Huff V et al. Wt1 directs the lineage specification of sertoli and granulosa cells by repressing Sf1 expression. *Development* 2017; **144**:44–53.
30. Gao F, Zhang J, Wang X, Yang J, Chen D, Huff V, Liu YX. Wt1 functions in ovarian follicle development by regulating granulosa cell differentiation. *Hum Mol Genet* 2014; **23**:333–341.
31. Hanrahan AJ, Schultz N, Westfal ML, Sakr RA, Giri DD, Scarperi S, Janakiraman M, Olvera N, Stevens EV, She QB, Aghajanian C, King TA et al. Genomic complexity and AKT dependence in serous ovarian cancer. *Cancer Discov* 2012; **2**:56–67.
32. Flesken-Nikitin A, Choi KC, Eng JP, Shmidt EN, Nikitin AY. Induction of carcinogenesis by concurrent inactivation of p53 and Rb1 in the mouse ovarian surface epithelium. *Cancer Res* 2003; **63**:3459–3463.